iScience

CellPress

Article

Structure of Human Mitochondrial Translation Initiation Factor 3 Bound to the Small Ribosomal Subunit

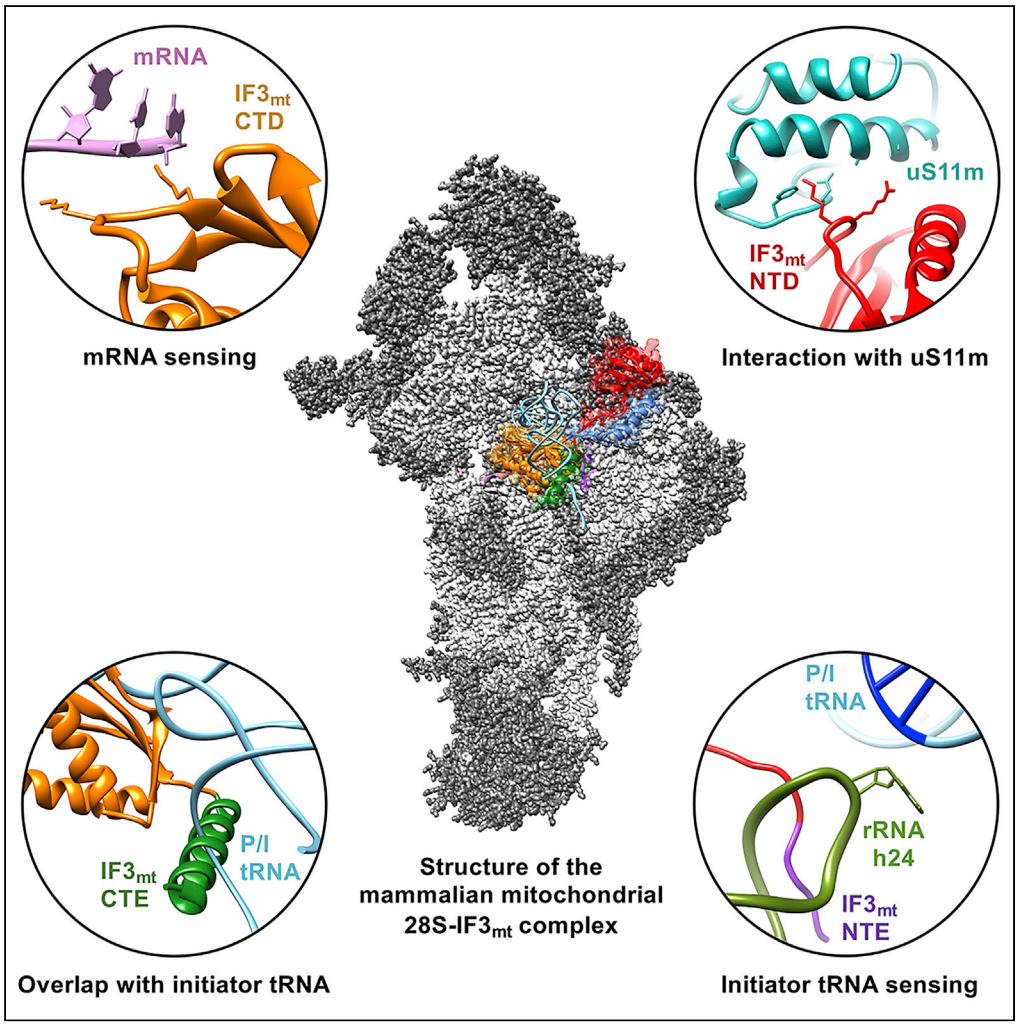

Ravi K. Koripella, Manjuli R. Sharma, Md. Emdadul Haque, Paul Risteff, Linda L. Spremulli, Rajendra K. Agrawal

rajendra.agrawal@health.ny.gov

HIGHLIGHTS

High-resolution cryo-EM study of the mammalian 28S mitoribosome-IF3$_{mt}$ complex

Interaction between the 28S and IF3$_{mt}$'s NTD explains NTD's unusual high affinity

Provides insights into role of IF3$_{mt}$'s N-terminal extension in initiator tRNA binding

Provides insights into roles of IF3$_{mt}$'s CTD and C-terminal extension in mRNA sensing

DATA AND SOFTWARE AVAILABILITY

6NF8
6NEQ

Koripella et al., iScience *12*, 76–86
February 22, 2019
https://doi.org/10.1016/j.isci.2018.12.030

iScience

CellPress

Article

Structure of Human Mitochondrial Translation Initiation Factor 3 Bound to the Small Ribosomal Subunit

Ravi K. Koripella,[1] Manjuli R. Sharma,[1] Md. Emdadul Haque,[2,4] Paul Risteff,[1,5] Linda L. Spremulli,[2] and Rajendra K. Agrawal[1,3,6,*]

SUMMARY

The human mitochondrial translational initiation factor 3 ($IF3_{mt}$) carries mitochondrial-specific amino acid extensions at both its N and C termini (N- and C-terminal extensions [NTE and CTE, respectively]), when compared with its eubacterial counterpart. Here we present 3.3- to 3.5-Å-resolution cryoelectron microscopic structures of the mammalian 28S mitoribosomal subunit in complex with human $IF3_{mt}$. Unique contacts observed between the 28S subunit and N-terminal domain of $IF3_{mt}$ explain its unusually high affinity for the 28S subunit, whereas the position of the mito-specific NTE suggests NTE's role in binding of initiator tRNA to the 28S subunit. The location of the C-terminal domain (CTD) clarifies its anti-association activity, whereas the orientation of the mito-specific CTE provides a mechanistic explanation for its role in destabilizing initiator tRNA in the absence of mRNA. Furthermore, our structure hints at a possible role of the CTD in recruiting leaderless mRNAs for translation initiation. Our findings highlight unique features of $IF3_{mt}$ in mitochondrial translation initiation.

INTRODUCTION

Mitochondria are believed to have originated from the α-proteobacteria following an endosymbiotic event, in which the latter was engulfed by a primitive eukaryotic host cell (Gray et al., 2001). Although mitoribosomes have retained several structural and functional similarities from their bacterial ancestors, they acquired several novel features. One remarkable difference is the considerable truncation of the rRNAs in the mitoribosomes compared with their bacterial counterparts (Anderson et al., 1981). However, the loss of rRNA is partially compensated for by the acquisition of several mitochondrial-specific ribosomal proteins and extensions and/or insertions in the ribosomal proteins that have bacterial homologs (Amunts et al., 2015; Brown et al., 2014; Greber et al., 2014, 2015; Kaushal et al., 2014; Sharma et al., 2003). Although the overall steps of protein synthesis in mammalian mitochondria appear to be similar to those in bacteria, there are several key differences in terms of the interaction of mitoribosome with the mRNAs, the tRNAs, and the mitochondrial translational factors (Christian and Spremulli, 2012; Lightowlers et al., 2014; Sharma et al., 2013).

Translation initiation in bacteria has been widely explored through biochemical and structural studies, and the roles of all the three canonical bacterial initiation factors IF1, IF2, and IF3 are well established. All three IFs are essential for translation initiation in bacteria (Boelens and Gualerzi, 2002), whereas in mammalian mitochondria, homologs of only two bacterial factors, $IF2_{mt}$ and $IF3_{mt}$, have been identified (Koc and Spremulli, 2002; Spencer and Spremulli, 2005). However, a mito-specific 37-amino-acid (aa)-long insertion domain in $IF2_{mt}$ has been proposed to mimic the function of bacterial IF1 during translation initiation in mammalian mitochondria (Gaur et al., 2008; Kummer et al., 2018; Yassin et al., 2011). In mimicking the function of IF1, the insertion domain in $IF2_{mt}$ sterically blocks the binding of initiator tRNA to the ribosomal A site (Yassin et al., 2011). $IF2_{mt}$ has been biochemically characterized *in vitro*, and it was shown to stimulate the binding of formyl-methionyl (fMet)-$tRNA^{fMet}$ to the small (28S) ribosomal subunit in the presence of mRNA (Ma and Spremulli, 1995; Spencer and Spremulli, 2005).

In bacteria, IF3 has been assigned multiple functions including discriminating elongator tRNAs from initiator tRNAs (Hartz et al., 1990; Hussain et al., 2016), promoting the dissociation of fMet-$tRNA^{fMet}$ at AUG codons on leaderless mRNAs (Tedin et al., 1999), and preventing the premature association of the 50S subunit with the 30S subunit until the formation of a proper pre-initiation complex (Hussain et al., 2016; Kaji

[1]Division of Translational Medicine, Wadsworth Center, New York State Department of Health, Albany, NY 12201-0509, USA

[2]Department of Chemistry, Campus Box 3290, University of North Carolina, Chapel Hill, NC, USA

[3]Department of Biomedical Sciences, School of Public Health, University at Albany, SUNY, Albany, NY, USA

[4]Present address: Audentes Therapeutics, CMC Analytical Development, 201 Gateway Blvd, South San Francisco, CA 94080, USA

[5]Present address: Charles River Laboratories Inc., 4025 Stirrup Creek Dr # 150, Durham, NC 27703, USA

[6]Lead Contact

*Correspondence: rajendra.agrawal@health.ny.gov

https://doi.org/10.1016/j.isci.2018.12.030

et al., 2001; Zavialov et al., 2005). IF3 has also been implicated in the ribosome recycling process, although its exact role in this process has not been established. Bacterial IF3 has been reported to actively participate in the ribosomal subunit splitting event together with EF-G and RRF (Hirokawa et al., 2002; Kaji et al., 2001). At the same time, it has been suggested to act passively by removing the deacylated tRNA from the 30S subunit after the latter is dissociated from the 70S particle (Karimi et al., 1999; Zavialov et al., 2005). $IF3_{mt}$ stimulates the formation of initiation complexes at the 5′-terminal start codon on leaderless mRNAs that are specific to mitochondria (Christian and Spremulli, 2010). Unlike its bacterial homolog, which acts as an anti-association factor, $IF3_{mt}$ actively splits the 55S mitoribosomes by shifting the equilibrium between the 55S monosome and its two subunits (small 28S and large 39S) toward subunit dissociation (Koc and Spremulli, 2002). $IF3_{mt}$ has also been shown to dissociate the initiator fMet-$tRNA^{fMet}$ from the 28S subunit in the absence of mRNA (Bhargava and Spremulli, 2005; Haque and Spremulli, 2008). Using an *E. coli* translation system, $IF3_{mt}$ has been shown to promote the binding of initiator tRNAs containing the conserved 3GC base pairs in the anticodon stem (Ayyub et al., 2017).

Mammalian $IF3_{mt}$ has diverged considerably from its bacterial counterparts and retains only 20% to 25% sequence homology (Koc and Spremulli, 2002). Although the basic domain organization is very similar to bacterial IF3 comprising N- and C-terminal domains that are connected through a flexible linker, the mammalian mitochondrial factor has additional ~30-aa-long extensions flanking both its termini (Bhargava and Spremulli, 2005; Haque et al., 2008; Koc and Spremulli, 2002). Deletions of these extensions have negative effects on the function of $IF3_{mt}$ during the initiation phase. Deletion of the C-terminal extension (CTE) renders the factor ineffective in destabilizing the incorrect initiation complexes, whereas deletion of the N-terminal extension (NTE) significantly increases the affinity of $IF3_{mt}$ for the 39S subunit (Bhargava and Spremulli, 2005; Haque and Spremulli, 2008). To further investigate the function of $IF3_{mt}$ in mitochondrial translational initiation and to understand the precise role of the mito-specific NTE and CTE, we have determined the cryoelectron microscopic (cryo-EM) structures of the human $IF3_{mt}$ bound to the bovine (*Bos taurus*) 28S subunit at 3.3 to 3.5 Å resolution.

RESULTS AND DISCUSSION

Position of $IF3_{mt}$ on the 28S Mitoribosomal Subunit

We obtained a complex between the bovine 28S subunit and the human $IF3_{mt}$ by incubating the two components at 37°C for 5 min and obtained a 3D cryo-EM structure at 3.1 Å resolution (Figures S1C, S1D, and S2A). The map showed a strong density for readily recognizable body and platform domains of the subunit, whereas the density for the head domain was relatively weak, suggesting a conformational heterogeneity in the head domain. Moreover, a density corresponding to $IF3_{mt}$ could be readily identified in the map. To improve the density for the head domain, the dataset of 198,355 selected images was subjected to 3D classification, which yielded two major $IF3_{mt}$-bound 28S mitoribosomal classes and a minor class that contained unusable images (Figure S1C). When the cryo-EM maps of the two $IF3_{mt}$-bound classes were superimposed, the head regions of the two 28S subunit maps show relative rotation. The 28S-$IF3_{mt}$ complex that has conformation similar to that of the 28S subunit in the published human and porcine 55S mitochondrial ribosomal structures (Amunts et al., 2015; Greber et al., 2015) is referred to as Class I (resolution 3.5 Å) (Figures S2B and S3A; Table S1), and the class with conformational deviation is referred to as Class II (resolution 3.3 Å) (Figures S2C and S3B; Table S1). Between the two classes, rotation of the head domain along the 12S rRNA helix 28 (h28, base G524 served as the pivotal point of rotation) was estimated to be around 4.5° (Figure S3C). A similar type of head movement, generally known as head swiveling, has been reported previously in bacterial (Ratje et al., 2010; Schuwirth et al., 2005) and mammalian mitochondrial ribosomes (Amunts et al., 2015).

In both Class I and Class II maps a well-defined density, corresponding to two globular domains that were separated by a narrow helical region, could be readily identified as $IF3_{mt}$ (Figures 1A–1C and S4). However, despite substantial head movement, the position of $IF3_{mt}$ in the two classes remained almost unchanged (Figure S5A). Most of the interactions and conclusions presented in the upcoming sections of this article are based on Class II 28S-$IF3_{mt}$ complex, as it contained a better resolved $IF3_{mt}$ than in Class I and enabled near-atomic interpretations. Human $IF3_{mt}$ is composed of 278 aa where the first 31 residues constitute the mitochondrial target sequence (MTS) (Bhargava and Spremulli, 2005; Haque and Spremulli, 2008; Koc and Spremulli, 2002), a signal sequence necessary for the transport of $IF3_{mt}$ into the mitochondria. After the MTS is cleaved, the mature $IF3_{mt}$ is left with 247 aa that fold into two globular domains (Figures 1C and 1D). The overall binding position of $IF3_{mt}$ on the 28S subunit is consistent with the earlier published

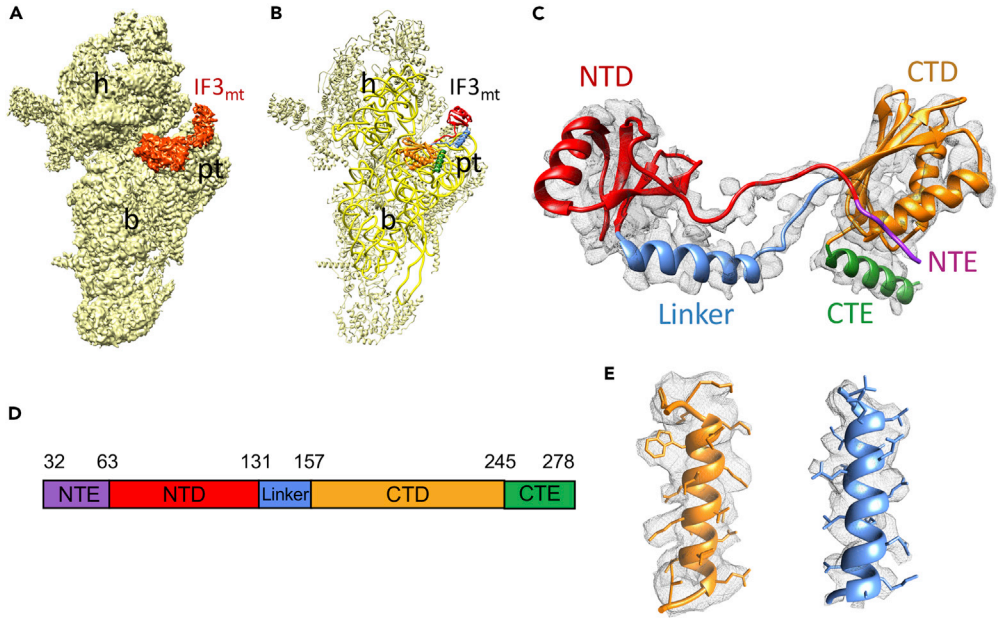

Figure 1. Cryo-EM Structure of the Mammalian Mitochondrial 28S-IF3$_{mt}$ Complex

(A) Three-dimensional cryo-EM map of the 28S mitoribosome-IF3$_{mt}$ complex, as viewed from the subunit's side that would face the large mitoribosomal subunit. The 28S subunit is shown in yellow, and the density corresponding to the IF3$_{mt}$ is shown in orange.

(B) Molecular interpretation of the cryo-EM map in (A). The 12S rRNA is displayed in bright yellow, whereas a lighter shade of yellow is used to mark the 28S ribosomal proteins (PDB ID: 3JD5). Landmarks of the 28S subunit: h, head; b, body; pt, platform.

(C) Completed model of IF3$_{mt}$ shown along with the corresponding cryo-EM density. Domains of IF3$_{mt}$ are color coded as in (D).

(D) Overall domain organization of the human IF3$_{mt}$.

(E) Some of the segments of IF3$_{mt}$ with better resolved densities.

cryo-EM reconstructions of bacterial IF3 in complex with the 30S subunit (Hussain et al., 2016; Julian et al., 2011; Lopez-Alonso et al., 2017; McCutcheon et al., 1999) and site-directed hydroxyl radical probing experiments on 30S-IF3 complexes (Dallas and Noller, 2001; Fabbretti et al., 2007). The NTD is made up of a single α helix and four β sheet strands, whereas the CTD is composed of a four-stranded β sheet that is packed against two α helices (Figure 1C). The domains are connected through a helical linker region that confers conformational flexibility to both globular domains (Figure 1C). In the following sections, we describe the molecular interactions between the 28S subunit components and IF3$_{mt}$, starting with the NTD, linker, CTD, and finally, mito-specific NTE and CTE.

Interactions of the NTD

Of the two globular domains of IF3$_{mt}$, its NTD binds closer to the cliff of the 28S subunit platform, in a position similar to that of the NTD of IF3 in the eubacterial complex. However, despite having a structural fold similar to that in a bacterial IF3 (Figure S5B), the orientation of the NTD in the mitoribosome structure is significantly different from that observed in the published bacterial 30S-IF3 complex structures (Figure S5C). None of the reported bacterial structures show any interaction between the NTD of IF3 and the 30S subunit (Hussain et al., 2016; Lopez-Alonso et al., 2017). In the mitochondrial complex, the NTD of IF3$_{mt}$ is oriented much closer to the 28S small subunit than the NTD of IF3 in any of the three 30S-IF3 complexes. This orientation allows the NTD to make multiple interactions with the adjacent ribosomal components such as mitoribosomal protein (MRP) uS11 and 12S rRNA helix 23 (h23). Despite the slightly lower resolution of the NTD (Figure S4), some of its bulky aa side chains could be traced. Arg80 in the NTD of IF3$_{mt}$ is found in close proximity to Ala137 and Ala140 of uS11m, whereas the adjacent Lys81 of the NTD is positioned close to Glu118 and Phe120 of the same MRP (Figure 2A). Val78 from the loop region of the NTD contacts the sugar moeity of h23 nucleotide (nt) A333, and the adjacent Phe75 is located in the

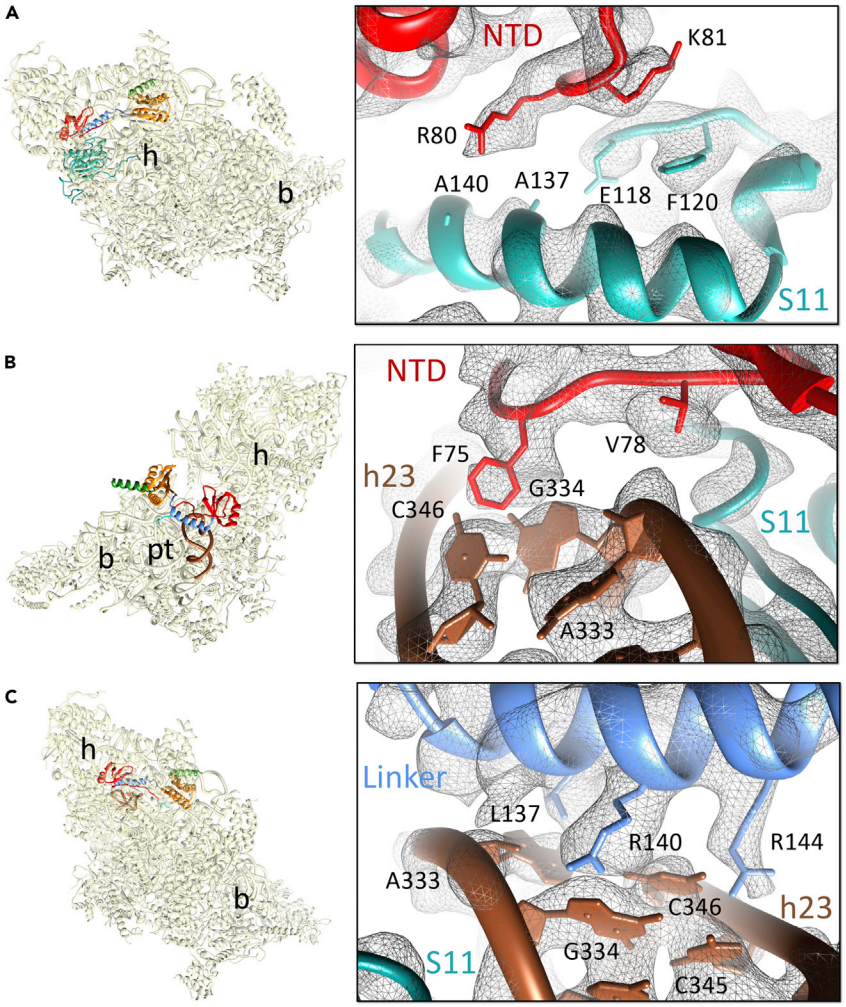

Figure 2. Interactions of the IF3$_{mt}$ NTD and the Linker Regions with the 28S Subunit

(A and B) (A) Interactions of the IF3$_{mt}$ NTD (red) with mitoribosomal protein S11 (cyan) and (B) 12S rRNA helix h23 (brown). (C) Contacts between the IF3$_{mt}$ linker region (blue) and h23 of the 12S rRNA (brown). Thumbnails to the left represent overlaid positions of the ligands relative to the overall orientation to the 28S subunit (yellow). Landmarks on the thumbnail: h, head; b, body; pt, platform.

vicinity of h23 nts G334 and C346 in an apparent stacking interaction (Figure 2B). It is highly likely that one of the major functions of the NTD of IF3$_{mt}$ is to provide additional anchoring points to enhance its affinity for the 28S subunit. This interpretation is consistent with the observation that the CTD in isolation can be readily displaced from the 28S subunit by the 39S subunit, whereas the full-length factor with the intact NTD binds much tighter and is difficult to displace from the 28S subunit (Haque and Spremulli, 2008). Furthermore, the NTD of IF3$_{mt}$ has been shown to bind independently to the 28S subunit with high affinity (Christian and Spremulli, 2012; Haque and Spremulli, 2008), whereas the NTD of its bacterial counterpart cannot interact with the 30S subunit without the presence of its CTD partner and the linker (Petrelli et al., 2001). Thus, unique interactions observed in our structure suggest a greater role for the IF3$_{mt}$ NTD in mitochondrial translation initiation than that of its counterpart in eubacterial translation.

Interactions of the Linker

The linker region connecting the NTD and CTD is located on the rim of the 28S platform such that it runs over h23 of the 12S rRNA toward the P-site. Other than acting as a physical link between the NTD and CTD of IF3, the precise role of the linker region is not known in bacterial IF3 (Petrelli et al., 2001). However, in

mitochondria the linker seems to enhance the affinities of both the NTD and the CTD for the 28S subunit (Haque and Spremulli, 2008). In bacteria, the only connection identified between the linker and the 30S ribosomal subunit is through a Tyr residue (Tyr75 according to *E. coli* numbering) that interacts with the C701 from h23 of the 16S rRNA (Hussain et al., 2016). Tyr75 of IF3 is highly conserved among bacteria and was suggested to play a crucial role in start codon discrimination and the selection of initiator tRNA (Hussain et al., 2016). Surprisingly, this important residue is not present in $IF3_{mt}$. Instead, we find that two Arg residues (Arg140 and Arg144) and a Leu137 residue in $IF3_{mt}$ anchor the linker to the 28S platform by making multiple interactions with the 12S rRNA nts A333, G334, C345, and C346 of h23 (Figure 2C). Both the Arg residues are conserved in mammalian $IF3_{mt}$ (Figure S6A) and could have evolved to compensate for the loss of a single Tyr residue in eubacterial IF3 that was capable of providing stacking interactions.

Interactions of the CTD

The CTD of $IF3_{mt}$ is positioned on the 28S platform in the vicinity of the P-site, and it interacts with several components of the 12S rRNA, including helices h24, h44, and h45. The rRNA nts from h24 provide the majority of the contact points for the CTD binding. Multiple nts from the apical loop of h24, including A424, G425, and U427 interact with the CTD residues Lys159, Glu160, Leu161, Ile162, Thr174, and Gln178 (Figures 3A and 3B). nts U914 and C915 from h44 provide additional contact points by interacting with Ile167 and Asp171, respectively, whereas G936 from h45 interacts with His170 and Thr174 of $IF3_{mt}$ CTD (Figures 3C and 3D). The majority of the aa residues that are involved in 28S-CTD interactions are conserved among human mitochondria and bacteria (Figure S6C) and are also reported in CTD-30S interactions in bacteria (Hussain et al., 2016). It should be noted that the sequence conservation between the human mitochondrial and bacterial IF3s is less than 25% (Koc and Spremulli, 2002). This kind of structural and functional conservation among two highly distinct kingdoms of life shows that although mitochondrial ribosomes diverged considerably from their bacterial ancestors, they retained key aa and nt residues to perform very specific functions.

In the 28S-$IF3_{mt}$ complex, the position of the CTD is such that it would prevent the joining of the 39S subunit with the 28S subunit by directly interfering with the formation of two of the conserved inter-subunit bridges, B2a and B2b. The formation of bridge B2a requires binding with its partner helix 69 (H69) from the 16S rRNA in the 39S subunit (Figure 3E), Bridge B2b engages h24 from the 28S subunit and H67 from the 39S subunit (Greber et al., 2015; Kaushal et al., 2014). The location of the CTD would also prevent docking of the mito-specific P-site finger (protein mL40) from the 39S subunit during 55S formation (Figure 3E). The CTD of $IF3_{mt}$ thus safeguards the 28S subunit until a proper pre-initiation complex composed of $IF2_{mt}$, mRNA, and initiator tRNA has been formed, a mechanism that has been well described for the bacterial system (Hussain et al., 2016).

Interactions of the Mito-Specific N- and C-Terminal Extensions

As described earlier, $IF3_{mt}$ possesses extensions on both its termini (Bhargava and Spremulli, 2005; Koc and Spremulli, 2002). The roles of these extensions during $IF3_{mt}$-mediated mitochondrial initiation has been characterized through biochemical and mutational studies (Ayyub et al., 2017; Bhargava and Spremulli, 2005; Haque et al., 2008; Haque and Spremulli, 2008; Koc and Spremulli, 2002), but the function of these extensions at the molecular level was not known. Structure of the 28S-$IF3_{mt}$ complex presented here has helped us to directly visualize the interactions of both the NTE and CTE with the 28S subunit components and has enabled us to interpret their functional roles in mitochondrial translational initiation.

Role of the NTE

Using bacterial translation system, it was previously reported that $IF3_{mt}$ plays a role in maintaining translational fidelity by recognizing initiator tRNAs possessing the conserved 3GC base pairs in the anticodon stem and the NTD of $IF3_{mt}$ was proposed to be an important contributor to this function (Ayyub et al., 2017). However, structures of the bacterial 30S-IF3 complexes did not place the NTD anywhere close enough to the anticodon stem of the initiator tRNA to allow a direct interaction (Hussain et al., 2016; Lopez-Alonso et al., 2017) that would support a role of the NTD in discriminating against the non-initiator tRNAs. Similarly, in our 28S-$IF3_{mt}$ structure, the core of the NTD would not be positioned close to the 3GC pairs of the initiator tRNA, suggesting that the role of NTD of $IF3_{mt}$ in tRNA discrimination could only be indirect (Figure 4A). It was proposed that binding of IF3 induces conformational changes in the small subunit, allowing the conserved 16S rRNA bases G1338 and A1339 (according to *E. coli* numbering) to recognize the 3GC base pairs of the initiator tRNA through A-minor interactions (Dallas and Noller, 2001). Subsequent mutational studies (Lancaster and Noller, 2005) and crystallographic structures of the

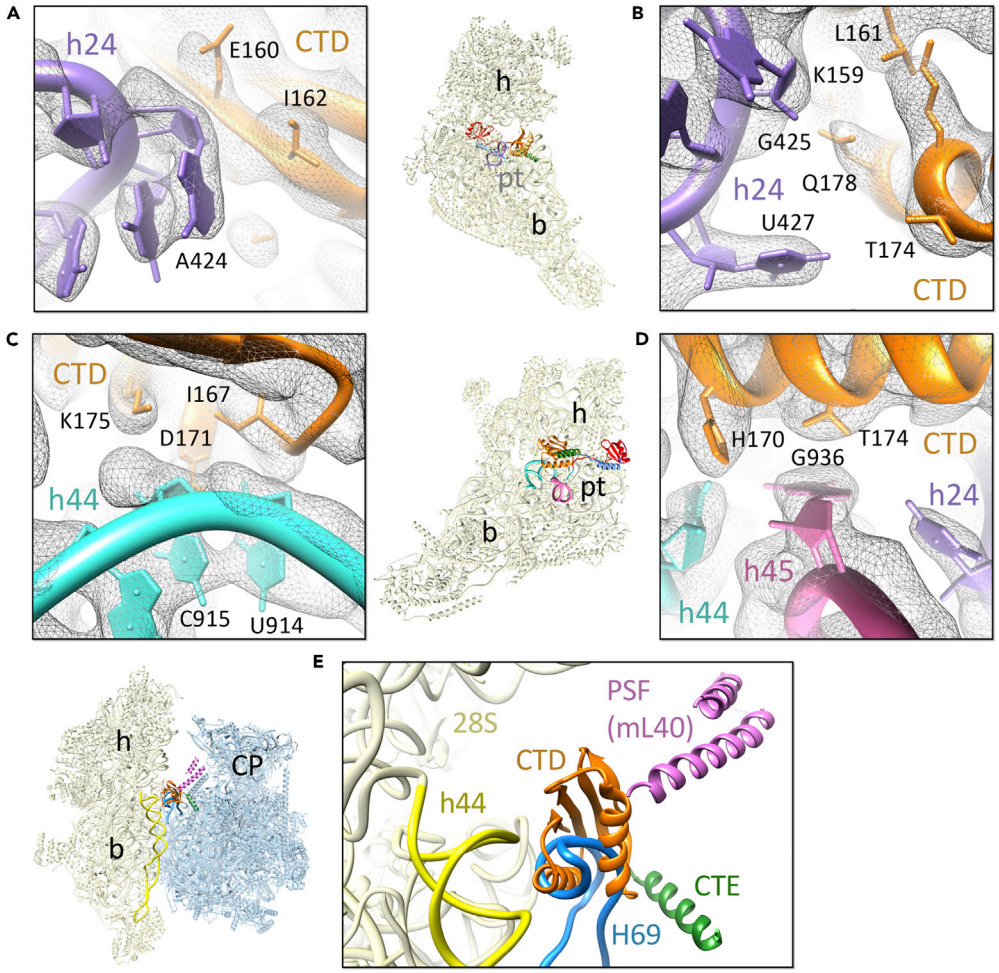

Figure 3. Interactions of the IF3$_{mt}$ CTD with the 28S Subunit and its Anti-association Property

(A–D) (A and B) The CTD (orange) provides major anchoring points for the stable binding of IF3$_{mt}$ by interacting with several 12S rRNA helices such as h24 (purple) and (C and D) h44 (cyan) and h45 (magenta). Thumbnails at the center represent overlaid positions of the ligands relative to the overall orientation to the 28S subunit (yellow).

(E) The CTD (orange) of IF3$_{mt}$ in its present conformation would prevent the association of 39S subunit with the 28S subunit by sterically blocking the formation of the central inter-subunit bridge, B2a, between h44 of the 28S subunit with H69 (blue), as well as docking of the mito-specific P-site finger (PSF, protein mL40, pink) from the large subunit. Landmarks on the thumbnail: CP, central protuberance of the large subunit; rest of the labels are the same as in Figure 2.

bacterial 70S ribosome complexes (Korostelev et al., 2006; Selmer et al., 2006), showing close proximity of G1338 and A1339 to the 3GC base pairs of the bound P-site tRNA, further cemented the importance of these rRNA residues in stabilizing the initiator tRNAs. Moreover, as the mammalian mitochondria carries a single tRNA^{Met} with 3GC base pairs (Anderson et al., 1981) that is involved in both translation initiation and elongation steps, its 3GC base pair feature appears to be relevant during the initiation step in the selection of tRNA^{Met} against the rest of the mitochondrial tRNAs.

Together with 3GC base pair interactions, additional interactions between the anticodon region and the ribosomal components have been proposed to be necessary for stable binding of the initiator tRNAs (Dallas and Noller, 2001). The highly conserved A790 located at the tip of h24 is known to interact with the anticodon region of the initiator tRNA and plays a crucial role during bacterial translation initiation (Fabbretti et al., 2007). In our Class II cryo-EM map, we found an additional low-resolution density close to the loop region of IF3$_{mt}$-NTD that would extend from the core of the NTD toward the ribosomal P-site and could be readily assigned to the NTE of IF3$_{mt}$ (Figures 1C and 4B). The low resolution of the density did not allow us to model the NTE at the side chain level, but the backbone of the polypeptide chain

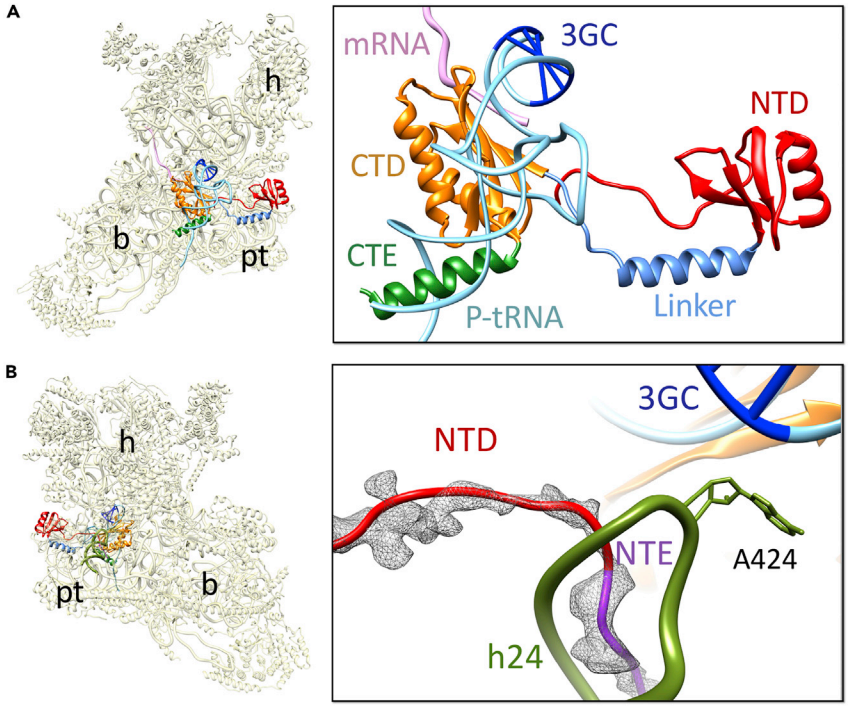

Figure 4. Relative Positions of NTD and NTE of $IF3_{mt}$ and Initiator tRNA

(A) The core of NTD (red) of $IF3_{mt}$ is situated away from the anticodon stem of the initiator tRNA (light blue) (M.R.S., R.K.K., N.K. Banavali, M.E.H., L.L.S., and R.K.A., unpublished data; Kummer et al., 2018) to interact with the conserved 3GC base pairs (dark blue) in the initiator tRNA. The mRNA (pink) is also shown. $IF3_{mt}$ domains are colored as in Figure 1.

(B) The NTD of $IF3_{mt}$ interacts with h24 (green) of 12S rRNA through its NTE (purple), whereas the h24 contacts the 3GC base pairs of the initiator tRNA with the help of a conserved adenine (A424). The cryo-EM density corresponding to the NTE (gray mesh) is also shown. Thumbnails to the left represent overlaid positions of the ligands relative to the overall orientation to the 28S subunit (yellow). Landmarks on the thumbnail: h, head; b, body; pt, platform.

could be traced. The NTE is positioned to make multiple interactions with h24 of the 12S rRNA thus aiding the high affinity of $IF3_{mt}$ for the small subunit. Most importantly, the NTE interacts with h24 carrying residue A424 (A790 in *E. coli*), and therefore, it is conceivable that the NTD through its NTE influences the binding of initiator tRNA in the P-site of the mitoribosome.

Role of the CTE

The high resolution of our structure allows us to model the CTE, except for the last 14 aa residues due to inconsistent local electron microscopic density. The CTE is composed of a single α helix, which is linked to the core CTD through a flexible loop region (Figures 1C and 5A). In the 28S-$IF3_{mt}$ complex, it is positioned away from the rim of the 28S platform and extends into what would be the inter-subunit side in a 55S mitoribosome complex. Interestingly, this is the only segment from the $IF3_{mt}$ that does not interact with any component of the 28S subunit. Although it does not have direct contacts with the 28S subunit, it is known to play an important role in mitochondrial translational initiation. When we superimposed our 28S-$IF3_{mt}$ structure on the structure of the mammalian mitochondrial 55S ribosome initiation complex comprising human $IF2_{mt}$ and initiator tRNA (M.R.S., R.K.K., N.K. Banavali, M.E.H., L.L.S., and R.K.A., unpublished date; Kummer et al., 2018), the CTE would prevent the binding of the initiator tRNA in the P-site position, as the α-helix of the CTE would be in steric clash with both the tRNA acceptor arm (Figure 5A) and domain VI of $IF2_{mt}$ (Figure 5B). Biochemical studies have suggested that $IF3_{mt}$ has the ability to destabilize the fMet-tRNA from the P-site of the 28S subunit in the absence of mRNA, but not if the 28S has a preloaded mRNA before the addition of fMet-tRNA (Bhargava and Spremulli, 2005; Christian and Spremulli, 2009). This unique function of $IF3_{mt}$ in sensing the precise order of events during mitochondrial initiation has not been reported in the bacterial system. Furthermore, the ability of $IF3_{mt}$ to dissociate the initiator tRNAs from the P-site in the absence of an mRNA is completely abolished if the CTE is removed from the factor (Bhargava and Spremulli, 2005; Christian and Spremulli, 2009). As our 28S-$IF3_{mt}$ complexes were devoid of an mRNA, the

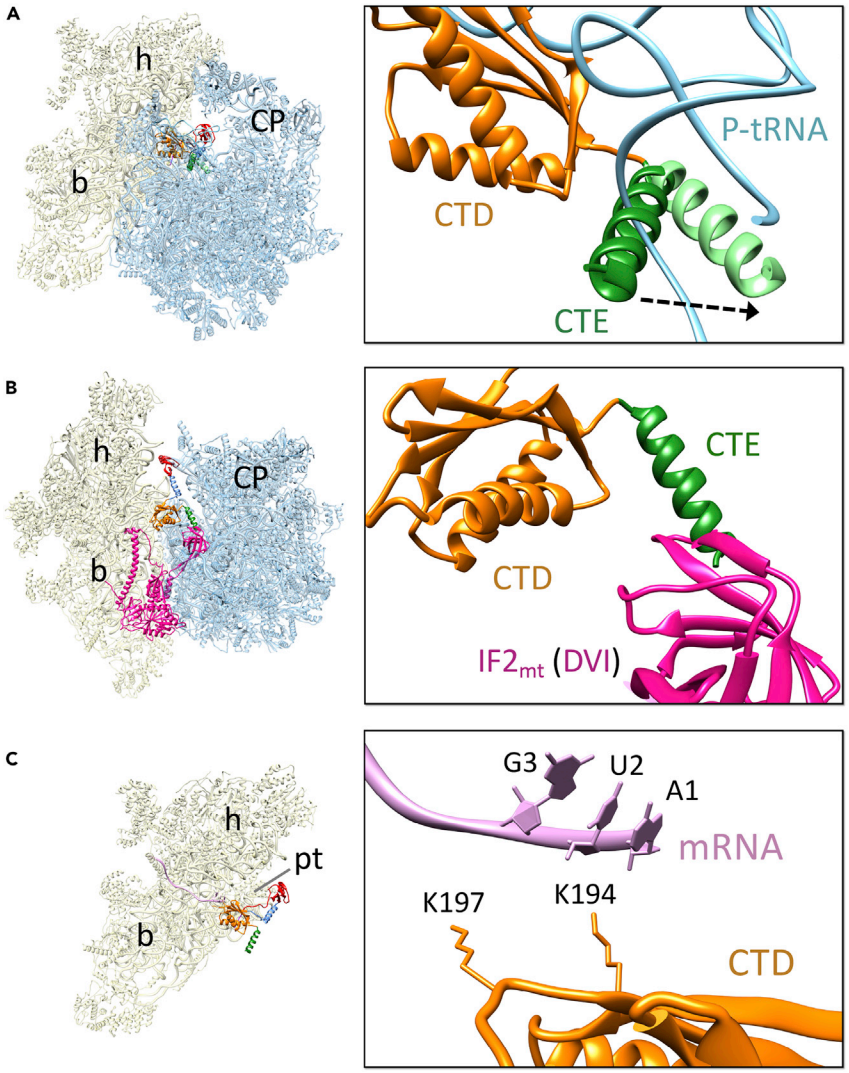

Figure 5. Interactions between CTE and the Acceptor Arm of Initiator tRNA, and between Conserved Lysine Residues of CTD and mRNA

(A) The CTE (dark green) in its current position would directly block the binding of initiator tRNA (light blue) (M.R.S., R.K.K., N.K. Banavali, M.E.H., L.L.S., and R.K.A., unpublished data; Kummer et al., 2018) in the absence of mRNA. Detection of mRNA by the CTD (orange) allows tRNA binding in the P-site by changing the conformation of its CTE. The loop connecting the CTE with the rest of CTD permits conformational flexibility, enabling the CTE to adopt multiple positions (depicted in light green) away from the acceptor arm of the initiator tRNA.

(B) Absence of mRNA in our 28S-IF3$_{mt}$ complex positions the CTE in an orientation that will also occlude the binding of domain VI of IF2$_{mt}$ (dark pink).

(C) The CTD (orange) of IF3$_{mt}$ is positioned on the 28S subunit with two of its conserved lysines (K194 and K197) oriented toward the bound mRNA (light pink). Thumbnail to the left depicts an overall orientation of the 55S mitoribosome, with 28S (yellow) and 39S (blue) subunits, and overlaid positions of ligands. Landmarks on the thumbnail: 28S subunit: h, head; b, body; pt, platform; 39S subunit: CP, central protuberance.

CTE is positioned in such a way that no tRNA binding would be allowed in the P-site. Without its CTE, the CTD alone would not be able to provide such steric hindrance to the P-site tRNA accommodation, explaining why this mito-specific mechanism is not observed in bacterial translation initiation, where IF3 lacks the CTE.

Still the question remains how does IF3$_{mt}$ detect the presence of a bound mRNA and prevent the accommodation of the initiator tRNA in the absence of the mRNA. Our analysis of the ribosomal environment

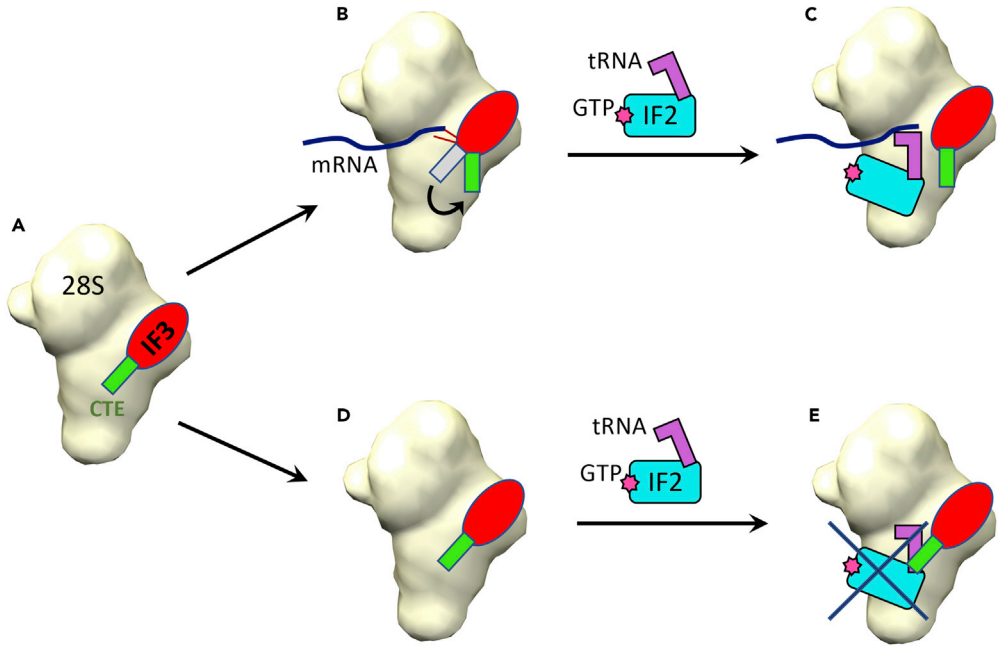

Figure 6. The Proposed Mechanism Depicting Roles of CTD and CTE in the Formation of Mammalian Translation Initiation Complex

(A) $IF3_{mt}$ binds to the 28S subunit, with its CTE in an extended position, as observed in our structure.

(B) If the mRNA is present, as probed by the conserved lysine residues in CTD of $IF3_{mt}$, the position of CTE (green) changes to accommodate binding of the $IF2_{mt}$·fMet-$tRNA_i$·GTP complex.

(C) 28S initiation complex formed.

(D and E) (D) If the mRNA is absent, the CTE (green) remains in an extended position to (E) sterically block the binding of the $IF2_{mt}$·fMet-$tRNA_i$·GTP complex.

surrounding the CTD of $IF3_{mt}$ helps providing an explanation for the ability of $IF3_{mt}$ to detect the presence of the mRNA on the 28S subunit. Two Lys residues (Lys194 and 197) from the CTD of $IF3_{mt}$ are oriented toward the bound mRNA when our structure is superimposed to the mammalian mitochondrial 55S-$IF2_{mt}$ initiation complex (Figure 5C) (M.R.S., R.K.K., N.K. Banavali, M.E.H., L.L.S, and R.K.A., unpublished data; Kummer et al., 2018). Both these Lys residues along with Lys195 and Gly196 residues (KKGK motif) are conserved among mammals (Figure S6B). One of these lysines (Lys194) is placed very close to the nts A1 and U2 from the bound mRNA. It is worth mentioning that the KKGK motif is substituted by a highly conserved FRGR motif in the bacterial factor and the second Arg (Arg133 according to *E. coli* numbering) was found to interact with the +4 base of the bound mRNA (Hussain et al., 2016). This conserved Arg residue was proposed to function either to position the mRNA in place or to aid in codon-anticodon discrimination (Hussain et al., 2016). We cannot rule out the possibility that these Lys residues (K194 and K197) might function to hold the start codon in position thereby compensating for the absence of the SD sequence in mitochondrial mRNAs (Temperley et al., 2010). Considering their high level of conservation, particularly among mammals (Figure S7), we assume that the CTD of $IF3_{mt}$ would sense the binding of mRNA with the help of these Lys residues and communicate the signal to the CTE. Once the presence of the mRNA has been detected, the orientation of the CTE would be altered to allow the initiator tRNA to enter the P-site (Figure 5A). The sturdy α helix of the CTE is connected to the CTD through a loop that would confer a high level of flexibility to the CTE, and its strategic positioning in the inter-subunit side, without any interaction with the rest of the 28S-$IF3_{mt}$ complex, would allow its multi-directional movements. Based on these findings, we propose a plausible model (Figure 6) that could also be tested to help understand the mechanism of translation initiation in many other systems wherein IF3 possesses a CTE and mRNAs are leaderless. For example, in mycobacteria about one-third of the mRNAs are leaderless (Shell et al., 2015) and the IF3 in this organism possesses a CTE (Figure S6D).

In conclusion, our study provides the high-resolution structure of the mitoribosome-bound human $IF3_{mt}$ and its mito-specific CTE and NTE, and their interactions with the mitoribosome, providing mechanistic

explanations for several unique biochemical properties of $IF3_{mt}$. Superimposition with the structure of the 55S·fMet-$tRNA_i$·$IF2_{mt}$ complex allows us to interpret the role of the CTD and its mito-specific CTE in destabilizing the initiator tRNA in the absence of mRNA. Future structural studies capturing the simultaneous presence of mRNA and $IF3_{mt}$ and mRNA, $IF3_{mt}$, and $IF2_{mt}$ on the 28S subunit should provide further insights into the mechanism of mitochondrial translation initiation.

Limitations of the Study

The model proposed in this study (Figure 6) is based on the structure of one of the functional states, i.e., binding of $IF3_{mt}$ to the 28S ribosomal subunit before mRNA and tRNA binding. Thus the proposed model is subject to test by solving the structure of additional states including mRNA, initiator tRNA, and $IF2_{mt}$.

METHODS

All methods can be found in the accompanying Transparent Methods supplemental file.

DATA AND SOFTWARE AVAILABILITY

Both cryo-EM maps of the 28S subunit of the mammalian (*Bos taurus*) mitochondrial ribosome bound to human IF3 have been deposited in the Electron Microscopy and PDB DataBank (wwPDB.org) under accession codes EMD-9362 and PDB ID 6NF8 for Complex I and under accession codes EMD-9358 and PDB ID 6NEQ for Complex II.

SUPPLEMENTAL INFORMATION

Supplemental Information includes Transparent Methods, seven figures, and one table and can be found with this article online at https://doi.org/10.1016/j.isci.2018.12.030.

ACKNOWLEDGMENTS

We acknowledge the use of the Wadsworth Center's and New York Structural Biology Center's (NYSBC's) EM facilities. NYSBC EM facilities are supported by grants from the Simons Foundation (349247), NYSTAR, the NIH (GM103310), and the Agouron Institute (F00316). We thank Kevin Elmore for help with purification of 28S subunits and $IF3_{mt}$ and ArDean Leith for help with computation. This work was supported by the NIH grants R01 GM61576 (to R.K.A.) and R01 GM32734 (to L.L.S.).

AUTHOR CONTRIBUTIONS

R.K.A. and L.L.S. conceived this study. M.E.H. performed biochemical experiments. P.R. prepared cryo-EM samples and helped with data collection. R.K.K. and M.R.S. performed image processing. R.K.K. and R.K.A. analyzed the data and wrote the manuscript.

DECLARATION OF INTERESTS

Authors declare no competing financial interest in this work.

Received: November 29, 2018
Revised: December 11, 2018
Accepted: December 27, 2018
Published: February 22, 2019

REFERENCES

Amunts, A., Brown, A., Toots, J., Scheres, S.H.W., and Ramakrishnan, V. (2015). Ribosome. The structure of the human mitochondrial ribosome. Science *348*, 95–98.

Anderson, S., Bankier, A.T., Barrell, B.G., de Bruijn, M.H., Coulson, A.R., Drouin, J., Eperon, I.C., Nierlich, D.P., Roe, B.A., Sanger, F., et al. (1981). Sequence and organization of the human mitochondrial genome. Nature *290*, 457–465.

Ayyub, S.A., Aswathy, S.L., Dobriyal, D., Aluri, S., Spremulli, L.L., and Varshney, U. (2017). Fidelity of translation in the presence of mammalian mitochondrial initiation factor 3. Mitochondrion *39*, 1–8.

Bhargava, K., and Spremulli, L.L. (2005). Role of the N- and C-terminal extensions on the activity of mammalian mitochondrial translational initiation factor 3. Nucleic Acids Res. *33*, 7011–7018.

Boelens, R., and Gualerzi, C.O. (2002). Structure and function of bacterial initiation factors. Curr. Protein Pept. Sci. *3*, 107–119.

Brown, A., Amunts, A., Bai, X.C., Sugimoto, Y., Edwards, P.C., Murshudov, G., Scheres, S.H.W., and Ramakrishnan, V. (2014). Structure of the large ribosomal subunit from human mitochondria. Science *346*, 718–722.

Christian, B.E., and Spremulli, L.L. (2009). Evidence for an active role of IF3mt in the initiation of translation in mammalian mitochondria. Biochemistry *48*, 3269–3278.

Christian, B.E., and Spremulli, L.L. (2010). Preferential selection of the 5′-terminal start codon on leaderless mRNAs by mammalian mitochondrial ribosomes. J. Biol. Chem. *285*, 28379–28386.

Christian, B.E., and Spremulli, L.L. (2012). Mechanism of protein biosynthesis in mammalian mitochondria. Biochim. Biophys. Acta *1819*, 1035–1054.

Dallas, A., and Noller, H.F. (2001). Interaction of translation initiation factor 3 with the 30S ribosomal subunit. Mol. Cell *8*, 855–864.

Fabbretti, A., Pon, C.L., Hennelly, S.P., Hill, W.E., Lodmell, J.S., and Gualerzi, C.O. (2007). The real-time path of translation factor IF3 onto and off the ribosome. Mol. Cell *25*, 285–296.

Gaur, R., Grasso, D., Datta, P.P., Krishna, P.D., Das, G., Spencer, A., Agrawal, R.K., Spremulli, L., and Varshney, U. (2008). A single mammalian mitochondrial translation initiation factor functionally replaces two bacterial factors. Mol. Cell *29*, 180–190.

Gray, M.W., Burger, G., and Lang, B.F. (2001). The origin and early evolution of mitochondria. Genome Biol. *2*, REVIEWS1018.

Greber, B.J., Boehringer, D., Leitner, A., Bieri, P., Voigts-Hoffmann, F., Erzberger, J.P., Leibundgut, M., Aebersold, R., and Ban, N. (2014). Architecture of the large subunit of the mammalian mitochondrial ribosome. Nature *505*, 515–519.

Greber, B.J., Bieri, P., Leibundgut, M., Leitner, A., Aebersold, R., Boehringer, D., and Ban, N. (2015). Ribosome. The complete structure of the 55S mammalian mitochondrial ribosome. Science *348*, 303–308.

Haque, M.E., Grasso, D., and Spremulli, L.L. (2008). The interaction of mammalian mitochondrial translational initiation factor 3 with ribosomes: evolution of terminal extensions in IF3mt. Nucleic Acids Res. *36*, 589–597.

Haque, M.E., and Spremulli, L.L. (2008). Roles of the N- and C-terminal domains of mammalian mitochondrial initiation factor 3 in protein biosynthesis. J. Mol. Biol. *384*, 929–940.

Hartz, D., Binkley, J., Hollingsworth, T., and Gold, L. (1990). Domains of initiator tRNA and initiation codon crucial for initiator tRNA selection by Escherichia coli IF3. Genes Dev. *4*, 1790–1800.

Hirokawa, G., Kiel, M.C., Muto, A., Selmer, M., Raj, V.S., Liljas, A., Igarashi, K., Kaji, H., and Kaji, A. (2002). Post-termination complex disassembly by ribosome recycling factor, a functional tRNA mimic. EMBO J. *21*, 2272–2281.

Hussain, T., Llacer, J.L., Wimberly, B.T., Kieft, J.S., and Ramakrishnan, V. (2016). Large-scale movements of IF3 and tRNA during bacterial translation initiation. Cell *167*, 133–144.e13.

Julian, P., Milon, P., Agirrezabala, X., Lasso, G., Gil, D., Rodnina, M.V., and Valle, M. (2011). The Cryo-EM structure of a complete 30S translation initiation complex from Escherichia coli. PLoS Biol. *9*, e1001095.

Kaji, A., Kiel, M.C., Hirokawa, G., Muto, A.R., Inokuchi, Y., and Kaji, H. (2001). The fourth step of protein synthesis: disassembly of the posttermination complex is catalyzed by elongation factor G and ribosome recycling factor, a near-perfect mimic of tRNA. Cold Spring Harb. Symp. Quant. Biol. *66*, 515–529.

Karimi, R., Pavlov, M.Y., Buckingham, R.H., and Ehrenberg, M. (1999). Novel roles for classical factors at the interface between translation termination and initiation. Mol. Cell *3*, 601–609.

Kaushal, P.S., Sharma, M.R., Booth, T.M., Haque, E.M., Tung, C.S., Sanbonmatsu, K.Y., Spremulli, L.L., and Agrawal, R.K. (2014). Cryo-EM structure of the small subunit of the mammalian mitochondrial ribosome. Proc. Natl. Acad. Sci. U S A *111*, 7284–7289.

Koc, E.C., and Spremulli, L.L. (2002). Identification of mammalian mitochondrial translational initiation factor 3 and examination of its role in initiation complex formation with natural mRNAs. J. Biol. Chem. *277*, 35541–35549.

Korostelev, A., Trakhanov, S., Laurberg, M., and Noller, H.F. (2006). Crystal structure of a 70S ribosome-tRNA complex reveals functional interactions and rearrangements. Cell *126*, 1065–1077.

Kummer, E., Leibundgut, M., Rackham, O., Lee, R.G., Boehringer, D., Filipovska, A., and Ban, N. (2018). Unique features of mammalian mitochondrial translation initiation revealed by cryo-EM. Nature *560*, 263–267.

Lancaster, L., and Noller, H.F. (2005). Involvement of 16S rRNA nucleotides G1338 and A1339 in discrimination of initiator tRNA. Mol. Cell *20*, 623–632.

Lightowlers, R.N., Rozanska, A., and Chrzanowska-Lightowlers, Z.M. (2014). Mitochondrial protein synthesis: figuring the fundamentals, complexities and complications, of mammalian mitochondrial translation. FEBS Lett. *588*, 2496–2503.

Lopez-Alonso, J.P., Fabbretti, A., Kaminishi, T., Iturrioz, I., Brandi, L., Gil-Carton, D., Gualerzi, C.O., Fucini, P., and Connell, S.R. (2017). Structure of a 30S pre-initiation complex stalled by GE81112 reveals structural parallels in bacterial and eukaryotic protein synthesis initiation pathways. Nucleic Acids Res. *45*, 2179–2187.

Ma, L., and Spremulli, L.L. (1995). Cloning and sequence analysis of the human mitochondrial translational initiation factor 2 cDNA. J. Biol. Chem. *270*, 1859–1865.

McCutcheon, J.P., Agrawal, R.K., Philips, S.M., Grassucci, R.A., Gerchman, S.E., Clemons, W.M., Jr., Ramakrishnan, V., and Frank, J. (1999). Location of translational initiation factor IF3 on the small ribosomal subunit. Proc. Natl. Acad. Sci. U S A *96*, 4301–4306.

Petrelli, D., LaTeana, A., Garofalo, C., Spurio, R., Pon, C.L., and Gualerzi, C.O. (2001). Translation initiation factor IF3: two domains, five functions, one mechanism? EMBO J. *20*, 4560–4569.

Ratje, A.H., Loerke, J., Mikolajka, A., Brunner, M., Hildebrand, P.W., Starosta, A.L., Donhofer, A., Connell, S.R., Fucini, P., Mielke, T., et al. (2010). Head swivel on the ribosome facilitates translocation by means of intra-subunit tRNA hybrid sites. Nature *468*, 713–716.

Schuwirth, B.S., Borovinskaya, M.A., Hau, C.W., Zhang, W., Vila-Sanjurjo, A., Holton, J.M., and Cate, J.H. (2005). Structures of the bacterial ribosome at 3.5 A resolution. Science *310*, 827–834.

Selmer, M., Dunham, C.M., Murphy, F.V.t., Weixlbaumer, A., Petry, S., Kelley, A.C., Weir, J.R., and Ramakrishnan, V. (2006). Structure of the 70S ribosome complexed with mRNA and tRNA. Science *313*, 1935–1942.

Sharma, M.R., Koc, E.C., Datta, P.P., Booth, T.M., Spremulli, L.L., and Agrawal, R.K. (2003). Structure of the mammalian mitochondrial ribosome reveals an expanded functional role for its component proteins. Cell *115*, 97–108.

Sharma, M.R., Kaushal, P.S., Gupta, M., Banavali, N.K., and Agrawal, R.K. (2013). Insights into structural basis of mammalian mitochondrial translation. In Translation in Mitochondria and Other Organelles, A.-M. Duchene, ed. (Springer), pp. 1–28.

Shell, S.S., Wang, J., Lapierre, P., Mir, M., Chase, M.R., Pyle, M.M., Gawande, R., Ahmad, R., Sarracino, D.A., Ioerger, T.R., et al. (2015). Leaderless transcripts and small proteins are common features of the mycobacterial translational landscape. PLoS Genet. *11*, e1005641.

Spencer, A.C., and Spremulli, L.L. (2005). The interaction of mitochondrial translational initiation factor 2 with the small ribosomal subunit. Biochim. Biophys. Acta *1750*, 69–81.

Tedin, K., Moll, I., Grill, S., Resch, A., Graschopf, A., Gualerzi, C.O., and Blasi, U. (1999). Translation initiation factor 3 antagonizes authentic start codon selection on leaderless mRNAs. Mol. Microbiol. *31*, 67–77.

Temperley, R.J., Wydro, M., Lightowlers, R.N., and Chrzanowska-Lightowlers, Z.M. (2010). Human mitochondrial mRNAs–like members of all families, similar but different. Biochim. Biophys. Acta *1797*, 1081–1085.

Yassin, A.S., Haque, M.E., Datta, P.P., Elmore, K., Banavali, N.K., Spremulli, L.L., and Agrawal, R.K. (2011). Insertion domain within mammalian mitochondrial translation initiation factor 2 serves the role of eubacterial initiation factor 1. Proc. Natl. Acad. Sci. U S A *108*, 3918–3923.

Zavialov, A.V., Hauryliuk, V.V., and Ehrenberg, M. (2005). Splitting of the posttermination ribosome into subunits by the concerted action of RRF and EF-G. Mol. Cell *18*, 675–686.

ISCI, Volume *12*

Supplemental Information

Structure of Human Mitochondrial Translation Initiation Factor 3 Bound to the Small Ribosomal Subunit

Ravi K. Koripella, Manjuli R. Sharma, Md. Emdadul Haque, Paul Risteff, Linda L. Spremulli, and Rajendra K. Agrawal

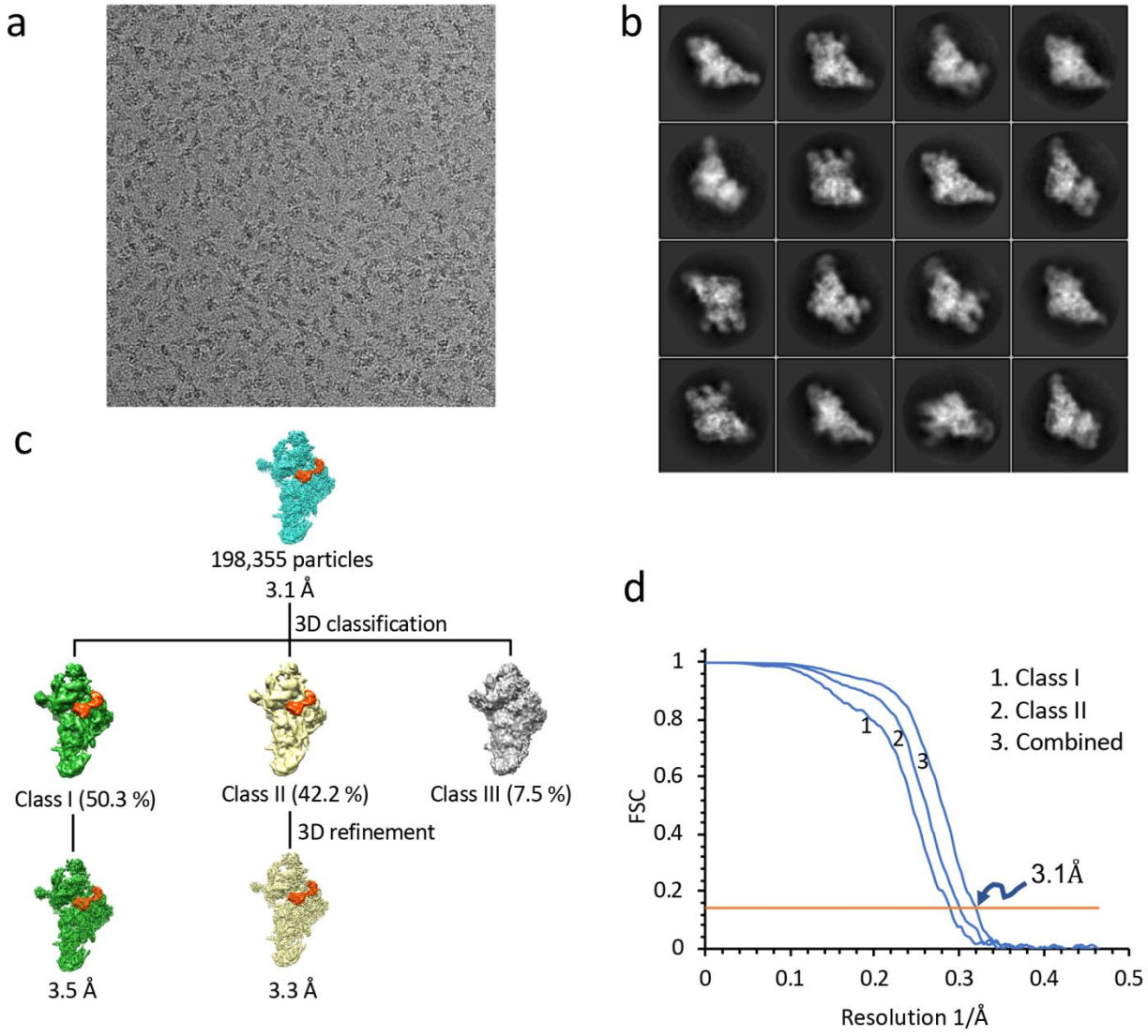

Figure. S1. Image processing of the 28S-IF3$_{mt}$ complex, Related to Figure 1 and Transparent Methods**.** (**a**) A typical electron micrograph showing the bovine mitochondrial 28S subunit in complex with human IF3$_{mt}$. (**b**) Representative two-dimensional (2D) class averages used in three-dimensional (3D) reconstructions. (**c**) Flow-chart showing results of 3D classification and refinements. A total of 198,355 particles corresponding to the selected 2D averages were refined to 3.1 Å. To remove conformational heterogeneity, the particles were subjected to 3D classification that yielded three different classes. After discarding the poorly aligned particles (Class III), particles corresponding to the other two classes were independently refined, to 3.5 Å (Class I), and 3.3 Å (Class II) (**d**) Fourier-shell correlation (FSC) curves of the final two maps that were used in our analysis.

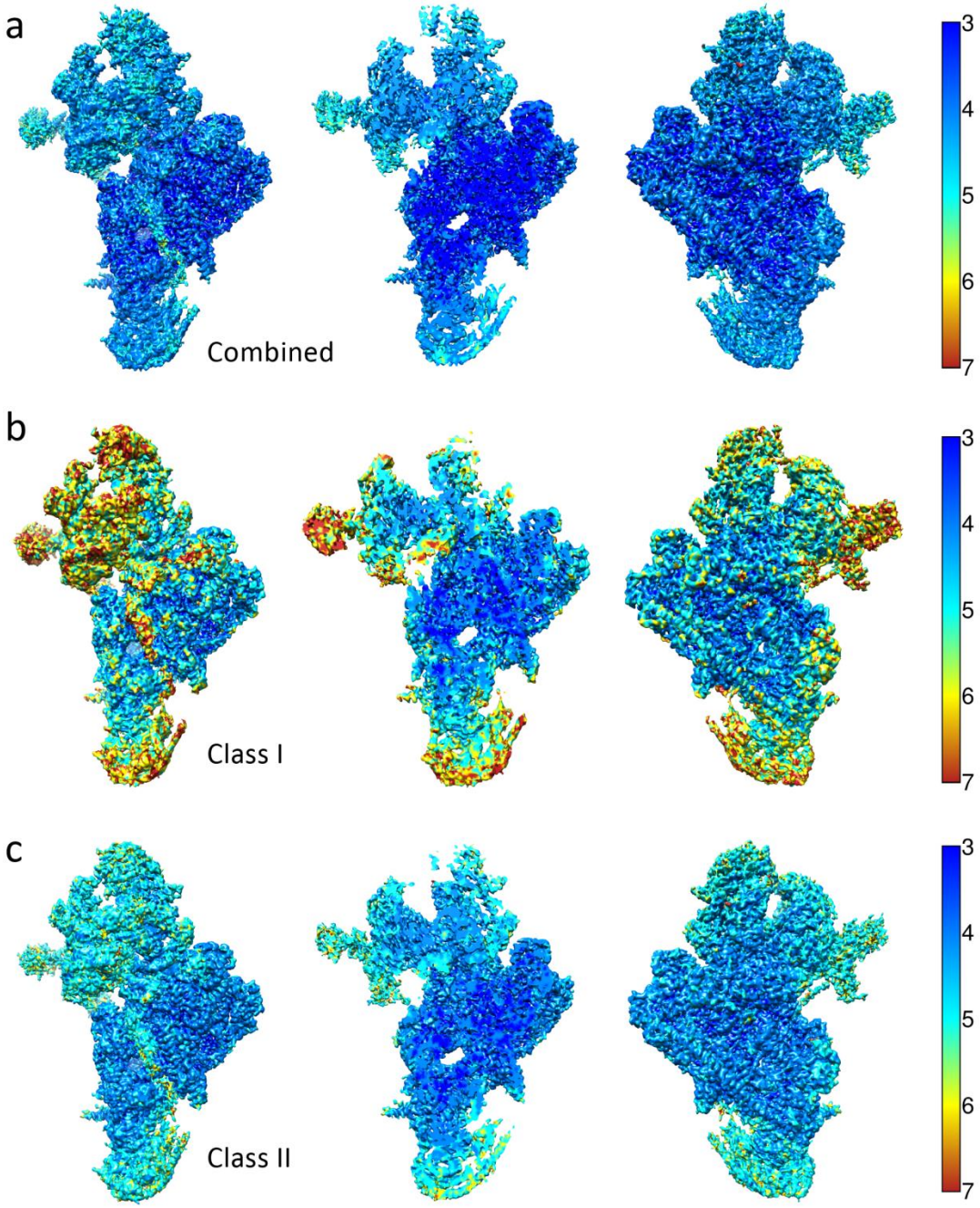

Figure. S2. Local resolution maps, Related to Figures 1, 2 and 3, and Transparent Methods**.** Local resolution for (**a**) the map obtained from full dataset, (**b**) Class I, and (**c**) Class II. Left panels show the local resolution maps as viewed from the subunit interface side, middle panels depict the core regions, after applying cutting planes, and right panels represent the view from the back side. Maps are color coded according to resolution bars shown on the extreme right.

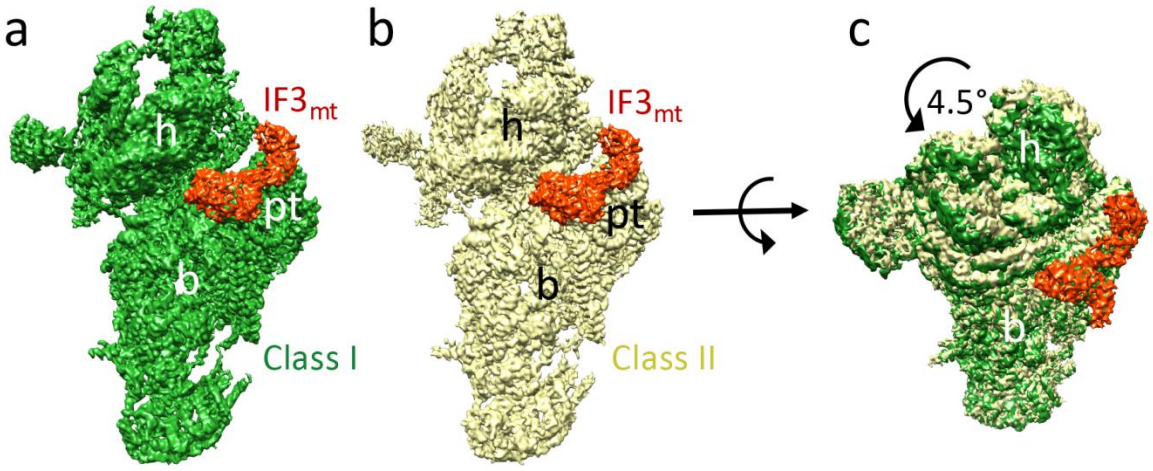

Figure. S3. Rotation of the 28S head relative to the platform region, Related to Figure 1**.** (**a**) Cryo-EM maps of class I (green) and (**b**) class II (yellow) with bound IF3$_{mt}$ (orange). Landmarks of the 28S subunit: h, head, b, body, and pt, platform. (**c**) Superimposition of class I with class II reveals an overall ~ 4.5 ° rotation of the 28S head in Class I, away from the platform region.

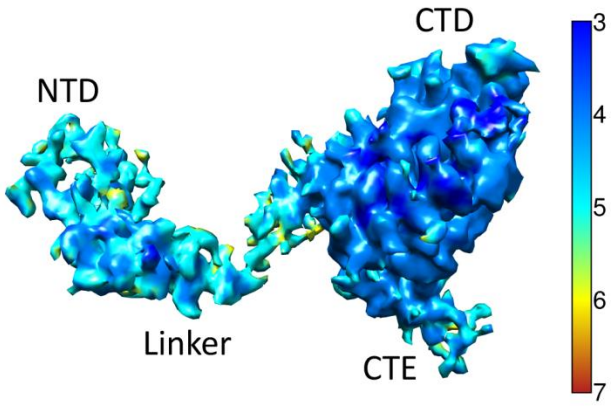

Figure. S4. Local resolution map of IF3$_{mt}$, Related to Figures 1 and 2**.** Local resolution for the density corresponding to IF3$_{mt}$ extracted from the cryo-EM map of the 28S-IF3$_{mt}$ Class II complex.

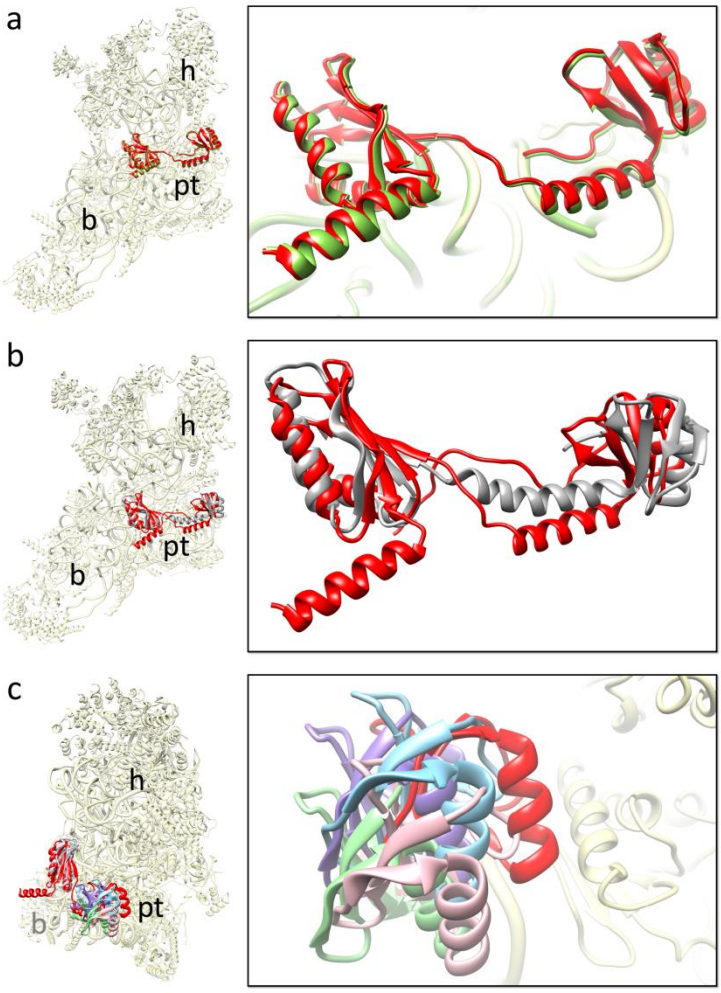

Figure. S5. Position of IF3$_{mt}$ NTD and CTD on the 28S subunit, Related to Figures 1 and 2**.** (**a**) The overall binding position of IF3$_{mt}$ in class I (green) and class II (red) remained almost identical, though the conformation of the 28S head domain is significantly different between these classes (Fig. S3). (**b**) Structures of the human IF3$_{mt}$ (red) and the bacterial IF3 (grey) (Hussain et al., 2016) superimposed. (**c**) The NTD of IF3$_{mt}$ (red) is positioned uniquely on the 28S subunit, as compared to the positions of NTD of the bacterial factor on the 30S subunit captured in four conformational states (lighter shades of green, purple, pink and blue) (Hussain et al., 2016; Lopez-Alonso et al., 2017). Thumbnails to the left represent overlaid positions of the ligands relative to the overall orientation to the 28S subunit (yellow). Landmarks on the thumbnail: h, head, b, body, and pt, platform.

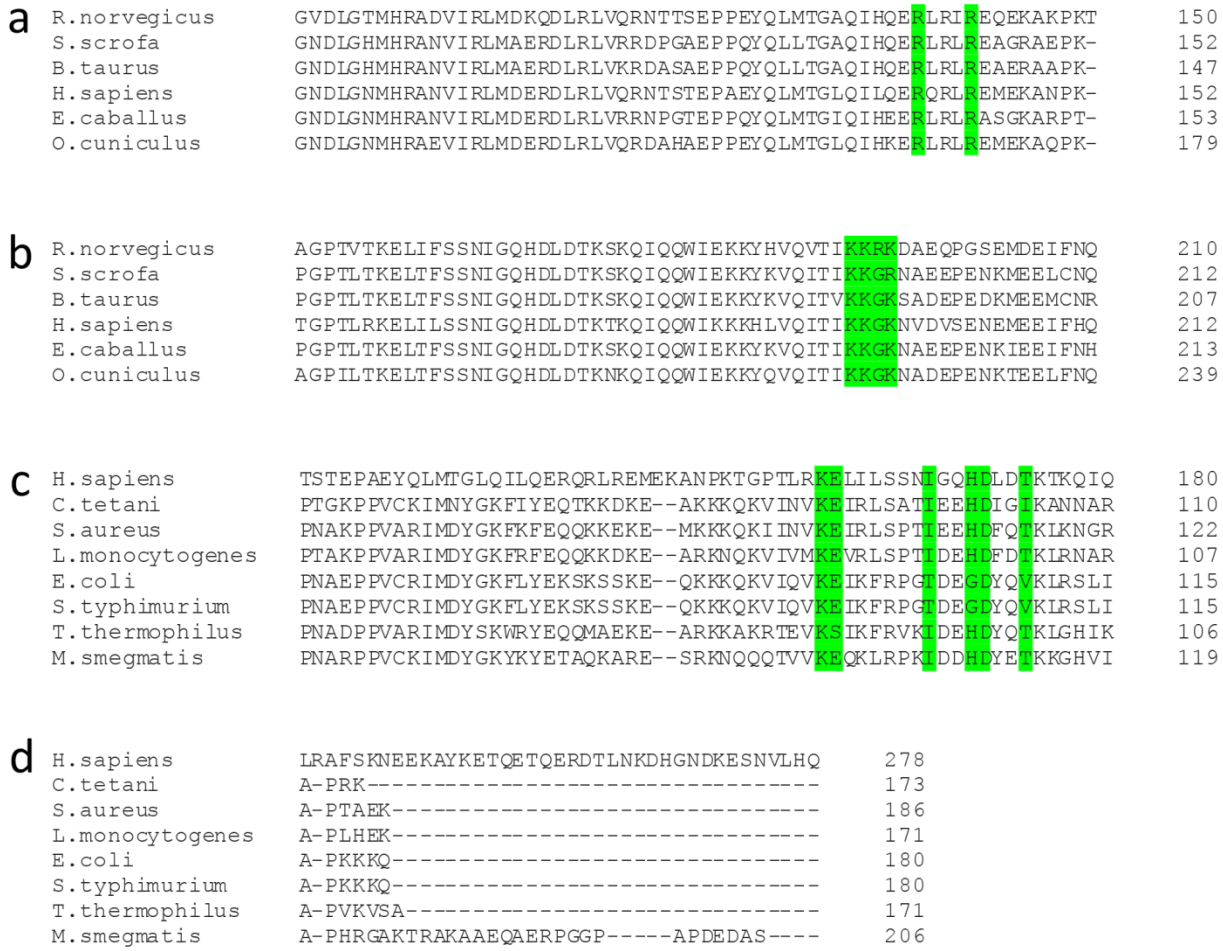

Figure. S6. Sequence alignment of mitochondrial IF3 homologues, Related to Figures 2, 3, and 6**.** Sequence alignment of select segments of (**a**, **b**) human $IF3_{mt}$ with other mammalian homologues, and (**c, d**) with bacterial homologues.

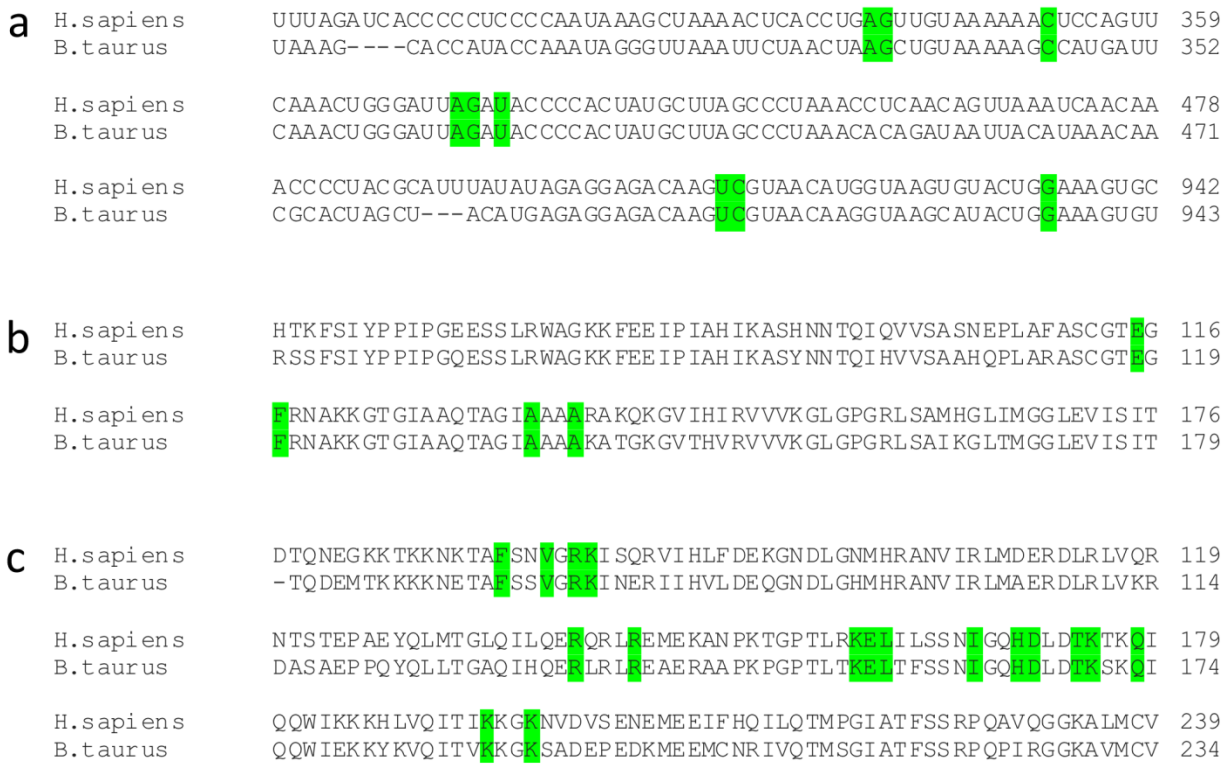

Figure. S7. Alignment of interacting segments of the 28S subunit components and IF3$_{mt}$ in human and bovine, Related to Figure 5**.** Select segments of (**a**) the 12S rRNA (**b**) MRP uS11 and (**c**) IF3$_{mt}$.

Table S1. Data Collection, Refinement and Model Validation, Related to Figures 1, 2, and 3, and Transparent Methods.

Description	**28S-IF3$_{mt}$ (Class I)**	**28S-IF3$_{mt}$ (Class II)**
Data collection and Refinement		
Microscope	FEI Titan Krios	
Voltage (kV)	300	
Pixel size (Å)	1.07	1.07
Defocus range (μm)	-1 to -3	-1 to -3
Average e^- dose per image ($e^-/Å^2$)	70.0	70.0
Software	RELION /cryoSPARC	RELION /cryoSPARC
Particles (initial)	198,355	198,355
Particles (final)	99,178	83,508
Symmetry	C1	C1
FSC-threshold	0.143	0.143
Resolution (Å)	3.48	3.32
Map-sharpening *B* factor ($Å^2$) overall	87.0	97.9
RMS deviations		
Bonds lengths (Å)	0.001	0.001
Bonds angles (°)	0.5	0.37
Molprobity clashscore	1.73 (88th)	1.70 (89th)
Clashscore, all atoms	3.23 (97th)	2.92 (98th)
Rotamer outliers (%)	0.06	0.04
Ramachandran plot		
Favored (%)	87.34	87.21
Outliers (%)	1.46	1.81
RNA		
Correct sugar puckers (%)	99.79	99.26
Angle outliers (%)	0.00	0.00
Bond outliers (%)	0.00	0.00
Good backbone conformations (%)	75.53	77.1
Model composition		
RNA bases Protein residues	952 5,482	952 5,482

Transparent Methods

Preparation of the 28S-IF3$_{mt}$ Complex: The mature form of human IF3$_{mt}$ was expressed and purified as described previously (Koc and Spremulli, 2002). Bovine mitochondrial 28S ribosomal subunits were prepared as described previously (Spremulli, 2007). Complexes containing IF3$_{mt}$ bound to 28S subunits were assembled in reaction mixtures (20 µL) containing 1 µM 28S subunits, 10 µM IF3$_{mt}$, 50 mM Tris-HCl, pH 7.6, 40 mM KCl, 7.5 mM $MgCl_2$, 10% glycerol, 2 mM dithiothreitol and 0.1 mM spermine. Reaction mixtures were incubated for 20 min at 25 ^{o}C, divided into 5 µL aliquots, fast-frozen in a dry ice isopropanol bath and stored at -70 ^{o}C. The amount of IF3$_{mt}$ bound to the 28S subunits was measured using a quantitative immuno dot blot using antibodies to bovine IF3$_{mt}$ as described previously (Haque and Spremulli, 2008). This analysis indicated that the complexes contained greater than 0.9 mol IF3$_{mt}$/mol 28S subunits. For cryo-EM analysis, the 28S-IF3$_{mt}$ complex was diluted to 100 nM with buffer containing 10 mM Tris-HCl, pH 7.6, 20 mM $MgCl_2$, 40 mM KCl, 1 mM DTT, 0.1 mM spermine and 5% glycerol, and then incubated for five min at 37°C prior to loading on the grids.

Cryo-Electron Microscopy and Image Processing: Home-made carbon was coated as a continuous layer (~ 50 Å thick) onto Quantifoil holey copper 1.2/1.3 grids, which were then glow-discharged for 30 s on a plasma sterilizer. After loading 4 µl of the sample to the grids, they were incubated for 15 s at 4°C and 100% humidity and then blotted for 4 s before flash-freezing into the liquid ethane using a Vitrobot (FEI). Data was acquired on a Titan Krios electron microscope equipped with a Gatan K2 summit direct-electron detecting camera at 300 KV. A defocus range of -1.0 to -3.0 µm was used at a calibrated magnification of 22,500 X, yielding a pixel size of 1.07 pixels Å on the object scale. A dose rate of 7 electrons per pixel per s and an exposure time of 10 s resulted in a total dose of 70 eÅ^{-2}. Out of the 2,435 micrographs that were collected, 2,095 were selected after determining their contrast transfer function (CTF) using CTFFIND3 (Rohou and Grigorieff, 2015). The data was then processed in Relion 2.0 (Scheres, 2012) where a total of 320,824 particles were picked using its autopick function. All the downstream steps including 2D classification, 3D

classification and 3D refinement were performed using CryoSPARC (Punjani et al., 2017). After reference-free 2D classification, 198,355 good particles were selected, and refined to a resolution of 3.1 Å. The map showed strong IF3$_{mt}$ density, but the 28S head region appeared to contain heterogeneity. Therefore, the dataset was subjected to an initial reference-based heterogenous 3D classification (Fig. S1). 3D classification yielded two major classes that turned out to be 28S-IF3$_{mt}$ complexes that showed conformational differences in their head regions and a minor class that contained mostly deformed ribosomal particles that could not be processed further. 3D refinement was performed on the two major classes that yielded a final resolution of 3.5 Å for Class I (99,178 particles) and 3.3 Å for Class II (83,508 particles) (Figs. S1 and S2).

Model Building: Coordinates from the published bovine 28S subunit (Kaushal et al., 2014; PDB ID: 3JD5) were docked independently as rigid bodies into the corresponding cryo-EM density maps of Class I and Class II using Chimera 1.11 (Pettersen et al., 2004). The models were subsequently refined and validated in PHENIX (Adams et al., 2010) using the real-space refinement function. Initial homology models for human IF3$_{mt}$ were obtained from the Robetta server (Kim et al., 2004). The homology models were then placed independently as rigid bodies into the region of density map corresponding to the IF3$_{mt}$ using Chimera 1.11 (Pettersen et al., 2004), and the model that showed optimal fitting were selected. Portions of the homology model that could not be explained by the cryo-EM density corresponding to IF3$_{mt}$ were modelled in Chimera, based on the recognizable secondary structural elements (SSEs) and bulky side-chains of the amino acids in the cryo-EM map. The mito-specific C-terminal extension (CTE) was built *de novo* in Chimera 1.11 (Pettersen et al., 2004), guided by SSEs and position of the side-chains, and Coot (Emsley et al., 2010). Low resolution in the region of the cryo-EM map corresponding to the mito-specific N-terminal extension (NTE) restricted us from modelling the complete NTE, but the carbon backbone. The final model was refined for optimal fitting into the density map and further validated in PHENIX (Adams et al., 2010). The statistics of EM reconstructions and molecular modeling is provided in Table S1.

Data Availability: Both cryo-EM maps of the 28S subunit of the mammalian (*Bos taurus*) mitochondrial ribosome bound to human IF3 have been deposited in the Electron Microscopy and PDB Data Bank (wwPDB.org) under accession codes EMD-9362 and PDB ID 6NF8 for Complex I and under accession codes EMD-9358 and PDB ID 6NEQ for Complex II.

Supplemental References:

Adams, P.D., Afonine, P.V., Bunkoczi, G., Chen, V.B., Davis, I.W., Echols, N., Headd, J.J., Hung, L.W., Kapral, G.J., Grosse-Kunstleve, R.W.*, et al.* (2010). PHENIX: a comprehensive Python-based system for macromolecular structure solution. Acta Crystallogr D Biol Crystallogr *66*, 213-221.

Emsley, P., Lohkamp, B., Scott, W.G., and Cowtan, K. (2010). Features and development of Coot. Acta Crystallogr D Biol Crystallogr *66*, 486-501.

Haque, M.E., and Spremulli, L.L. (2008). Roles of the N- and C-terminal domains of mammalian mitochondrial initiation factor 3 in protein biosynthesis. J Mol Biol *384*, 929-940.

Hussain, T., Llacer, J.L., Wimberly, B.T., Kieft, J.S., and Ramakrishnan, V. (2016). Large-Scale Movements of IF3 and tRNA during Bacterial Translation Initiation. Cell *167*, 133-144 e113.

Kaushal, P.S., Sharma, M.R., Booth, T.M., Haque, E.M., Tung, C.S., Sanbonmatsu, K.Y., Spremulli, L.L., and Agrawal, R.K. (2014). Cryo-EM structure of the small subunit of the mammalian mitochondrial ribosome. Proc Natl Acad Sci U S A *111*, 7284-7289.

Kim, D.E., Chivian, D., and Baker, D. (2004). Protein structure prediction and analysis using the Robetta server. Nucleic Acids Res *32*, W526-531.

Koc, E.C., and Spremulli, L.L. (2002). Identification of mammalian mitochondrial translational initiation factor 3 and examination of its role in initiation complex formation with natural mRNAs. J Biol Chem *277*, 35541-35549.

Lopez-Alonso, J.P., Fabbretti, A., Kaminishi, T., Iturrioz, I., Brandi, L., Gil-Carton, D., Gualerzi, C.O., Fucini, P., and Connell, S.R. (2017). Structure of a 30S pre-initiation complex stalled by GE81112 reveals structural parallels in bacterial and eukaryotic protein synthesis initiation pathways. Nucleic Acids Res *45*, 2179-2187.

Pettersen, E.F., Goddard, T.D., Huang, C.C., Couch, G.S., Greenblatt, D.M., Meng, E.C., and Ferrin, T.E. (2004). UCSF Chimera--a visualization system for exploratory research and analysis. J Comput Chem *25*, 1605-1612.

Punjani, A., Rubinstein, J.L., Fleet, D.J., and Brubaker, M.A. (2017). cryoSPARC: algorithms for rapid unsupervised cryo-EM structure determination. Nat Methods *14*, 290-296.

Rohou, A., and Grigorieff, N. (2015). CTFFIND4: Fast and accurate defocus estimation from electron micrographs. J Struct Biol *192*, 216-221.

Scheres, S.H. (2012). RELION: implementation of a Bayesian approach to cryo-EM structure determination. J Struct Biol *180*, 519-530.

Spremulli, L.L. (2007). Large-scale isolation of mitochondrial ribosomes from mammalian tissues. Methods Mol Biol *372*, 265-275.